Nano Energy 59 (2019) 285–294

Contents lists available at ScienceDirect

Nano Energy

journal homepage: www.elsevier.com/locate/nanoen

Full paper

Novel reduction of hysteresis loss controlled by strain memory effect in FeRh/PMN-PT heterostructures

Kaiming Qiao[a,b], Fengxia Hu[a,b,c,*], Yao Liu[a,b], Jia Li[a,b], Hao Kuang[a,b], Hongrui Zhang[a,b], Wenhui Liang[a,b], Jing Wang[a,b,d,*], Jirong Sun[a,b,c], Baogen Shen[a,b,c,*]

[a] Beijing National Laboratory for Condensed Matter Physics & State Key Laboratory of Magnetism, Institute of Physics, Chinese Academy of Sciences, Beijing 100190, PR China
[b] School of Physical Sciences, University of Chinese Academy of Sciences, Beijing 100049, PR China
[c] Songshan Lake Materials Laboratory, Dongguan, Guangdong 523808, PR China
[d] Fujian Institute of Innovation, Chinese Academy of Sciences, Fuzhou, Fujian 350108, PR China

ARTICLE INFO

Keywords:
Hysteresis loss
Strain memory effect
FeRh
PMN-PT
Refrigeration efficiency

ABSTRACT

As living standards increase, the energy consumption in refrigeration, such as air-conditioning and refrigerators, tremendously increases and intensifies global warming. As an alternative for the conventional vapor compression technique, solid state refrigeration based on magnetocaloric effect shows significant potential due to energy-saving and environmental-friendly properties. However, hysteresis loss is a longstanding problem seriously harming refrigeration efficiency. Here, we report novel enhancement of refrigeration efficiency controlled by strain memory effect in FeRh films grown on (011)-PMN-PT substrates. Utilizing nonvolatile strain triggered by a pulse electric field to engineer magnetization process of FeRh film, a nonvolatile large reduction of hysteresis loss, ~56%, is achieved, consequently effective refrigeration capacity increases to ~86%. The hysteresis loss can be expected to be eliminated and even turned out to be inverse through enhancing the strain memory effect. As a result, effective refrigeration capacity (RC_{effe}) can increase to a new height through introducing external mechanical work in a magnetic refrigeration cycle, and the ideal COP (coefficient-of-performance) would break through Carnot limit if only hysteresis loss and the contribution of mechanical work were considered.

1. Introduction

Conventional vapor compression refrigeration technique has been used everywhere in our daily life. However, the produced ozone depleting and/or greenhouse effects due to the usage of Freon and its substitutes seriously impact environment. Therefore, it is urgent to search an alternative technique especially after the new global climate Paris agreement [1]. Solid state refrigeration [2–11] based on magnetocaloric [2,10], electrocaloric [3,4], mechanocaloric effect [5,7] has attracted ever-increasing interest for its environmental-friendly and energy-saving superiority compared to conventional vapor compression technique. In the past two decades, the discovery of giant caloric materials, such as $Gd_5Si_{4-x}Ge_x$ [2], $La(Fe_{1-x}Si_x)_{13}$ [12,13], $MnFeP_{1-x}As_x$ [8], NiMnX [14,15], has indeed promoted the developing of solid state refrigeration technique.

As well known, FeRh is a giant magnetocaloric material [16,17] discovered earlier than the milestone material $Gd_5Si_2Ge_2$ [2]. The near-equiatomic FeRh alloys own a coupling between magnetic and structural order, hence a typical first-order transition accompanied with a volume expansion about 1% from antiferromagnetic (AFM) to ferromagnetic (FM) state occurs just above room temperature (around 350 K) [18]. This characteristic makes FeRh sensitive to various external stimulus, such as temperature, magnetic field [19], and strain [20], hence giant elastocaloric [21], and barocaloric effect [22] have been also reported in FeRh besides giant magnetocaloric effect (MCE) [16,17].

However, the usage of FeRh in a prototype has rarely been reported since its discovery [16] in 1990 because the large hysteresis loss and irreversibility hinder it to be as effective refrigerants. Hysteresis loss denotes heat leakage in a refrigeration cycle, which seriously reduces efficiency. Not merely in FeRh, many first order materials with giant MCE exhibit large hysteresis loss. Effectively decreasing the hysteresis loss is, therefore, a longstanding issue for the caloric materials. People dedicated lots of effort to reduce hysteresis loss, such as by doping [23], introducing porosity [24], or introducing hydrostatic pressure [14]. The remarkable work is the significant reduction of hysteresis loss in

* Corresponding authors.
E-mail addresses: fxhu@iphy.ac.cn (F. Hu), wangjing@iphy.ac.cn (J. Wang), shenbg@iphy.ac.cn (B. Shen).

https://doi.org/10.1016/j.nanoen.2019.02.044
Received 30 October 2018; Received in revised form 29 January 2019; Accepted 17 February 2019
Available online 19 February 2019

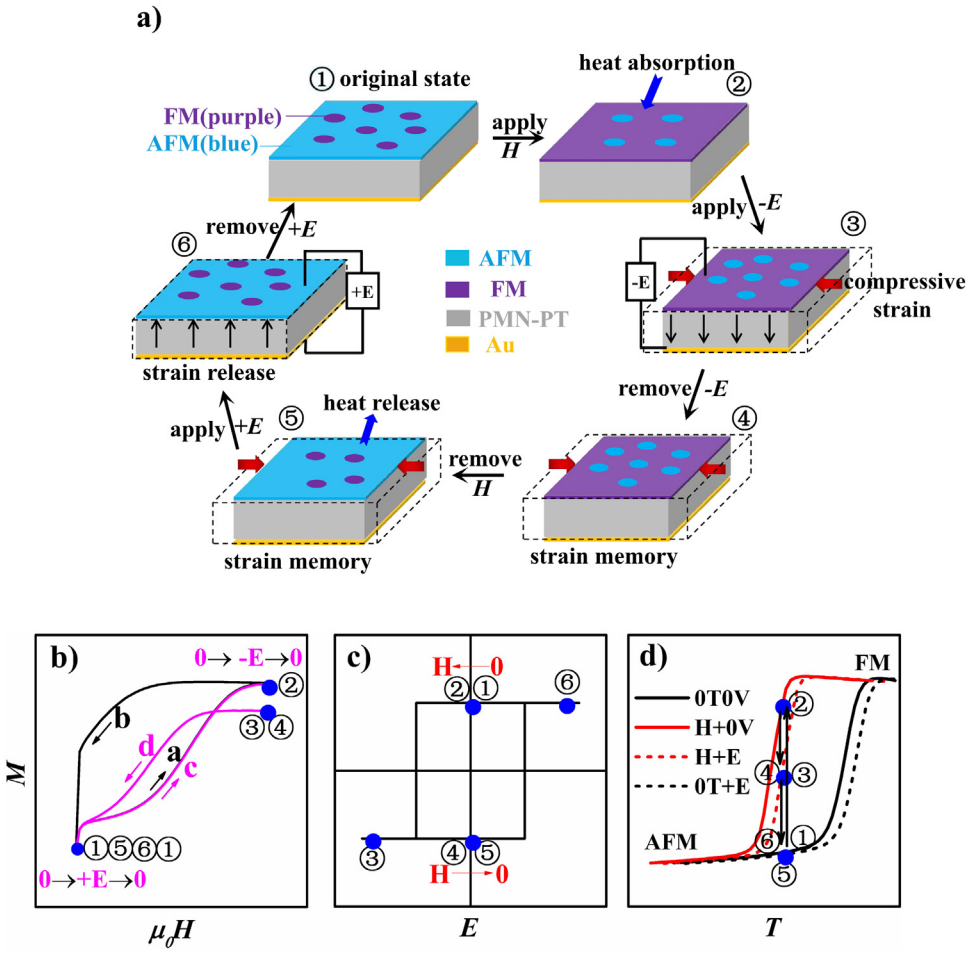

Fig. 1. Schematic of (a) refrigeration cycle, (b) *M-H* curves (after virgin cycle) with pulse ± *E* applied only at points of 0 T and *H*, and the corresponding (c) *M-E* curves and (d) *M-T* curves at magnetic fields of 0 T and *H*.

Heusler alloys NiMnCoIn proposed by utilizing multicaloric cycle combining magnetic field with hydrostatic pressure [14].

Although great successes in decreasing hysteresis loss have been achieved, most of the previously reported were focused on bulk samples. With the popularization of microelectronic devices, miniaturization of refrigeration devices has become an urgent demand of refrigeration technology. Compared to bulk, thin film has much broader application and richer physics owing to the size effect and the coupling with substrate. Recently, a magnetic-electric multicaloric cycle in a $FeRh/BaTiO_3$ heterostructure was proposed and a reduction of hysteresis loss had been observed [9] when a combined magnetic field and electric field was simultaneously applied during demagnetization process. However, the hysteresis loss firmly relies on the electric field, which would recover again when the driving electric field is removed. The continuously needed electric field during heat absorb/release (magnetization/demagnetization) process limits the design of a practical prototype, which makes the refrigeration cycling almost impossible when conductive fluid acts as heat transfer medium. Here, we report the nonvolatile control of hysteresis loss by strain memory effect in a FeRh thin film grown on a piezoelectric-type PMN-PT ferroelectric (FE) substrate. Utilizing the large strain memory effect provided by rhombohedral-to-orthorhombic (R-O) phase transformation upon bipoling along [011] direction, nonvolatile reduction of hysteresis loss is achieved in FeRh films by switching the magnetic state under a pulse electric field. The application of electric field is avoided during heat absorb/release (magnetization/demagnetization) process, which solves the bottleneck problem in technical design of electric-magnetic dual field cycle and makes the materials with large hysteresis loss practically possible as effective refrigerants. More attractively, as long as the strain memory effect can be large enough, the hysteresis loss is expected to be inverse, resulting in a novel enhancement of effective refrigeration capacity (RC_{effe}). The RC_{effe} can increase to a new height by utilizing mechanical work in a magnetic refrigeration cycle, and the ideal COP (coefficient-of-performance) would break through Carnot limit if only hysteresis loss and the contribution of mechanical work were considered.

2. Methods

2.1. Film growth

FeRh film was grown on (011)-oriented (1-x)PMN-xPT (PMN-PT) single crystal substrate (x = 0.30) by magnetron sputtering at 750 °C with a power of 30 W in an argon pressure of 0.2 Pa. The background vacuum pressure was 2×10^{-6} Pa. The films were annealed in situ for an hour at 750 °C and then cooled to room temperature in vacuum. FeRh target and PMN-PT substrates are both purchased commercially.

2.2. Measurement of magnetic properties

Au layers were vapor deposited on bottom side of FeRh/PMN-PT heterostructure as electrodes. The magnetic properties were measured using a superconducting quantum interference device (SQUID–VSM) with in situ electric fields applied across the thickness direction of FeRh/PMN-PT structure by a Keithley 6517B electrometer. The leakage current was below 5 nA under an electric field of 6 kV cm^{-1}. The pulse

width of electric field applied in the refrigeration cycle was 2 s.

2.3. Structure characterization under in situ electric fields

The crystal structure of PMN-PT substrates was characterized by X-ray diffraction performed in a Bruker AXS D8 discover X-ray diffractometer with Cu-Kα radiation with in situ electric fields applied across the thickness direction of FeRh/PMN-PT structure by a Keithley 6517B electrometer. The leakage current was below 5 nA under an electric field of 6 kV cm^{-1}. To understand the R-O transition and get information of in-plane lattice change along [100] direction, reciprocal space maps (RSMs) were measured around the (−222) reflection of PMN-PT substrate for different strain states produced by the pulse ± 6 kV cm^{-1}. Since the in-plane reciprocal vector components of reflections around the (−222) peak are parallel to the [100] direction, the lattice parameter along in-plane [100] direction can be deduced from the RSMs.

3. Results

3.1. Refrigeration cycle with strain memory effect

A refrigeration cycle involving the strain memory effect is detailedly schematized in Fig. 1a, and the full cycle has been demonstrated experimentally. Here, we suppose that the refrigeration cycle was carried out fast enough to be adiabatic in principle for all the steps. It is practically rational because the heat conductivity of PMN-PT substrate is small (thermal conductivity, κ ~ 1.2–1.3 Wm^{-1} K^{-1}) compared to metal (κ ~ 50–450 Wm^{-1} K^{-1}). Alternatively, a thermal barrier layer preserving strain coupling may be also considered to introduce between the substrates and films, which can avoid heat leakage from the FeRh film to PMN-PT substrate. Besides, advanced means can be put forward to solve this problem during refrigeration cycling. For example, if suitable materials can be chosen as heat transfer medium, the problem of heat leakage through substrate can be solved through careful designing the devices. Finite element simulation is performed by taking Cu, Ag, Au, graphene, Pt as heat transfer medium, respectively. Both simulation and experimental results illustrate that Cu is suitable as the heat transfer medium for FeRh grown on PMN-PT. The leakage heat through the substrate can be neglectable if Cu serves as the heat transfer medium (Details can be seen in Supporting information S4). For the typical FM materials grown on PMN-PT, the magnetization versus electric field (*M-E* curves) can be butterfly-like, loop-like, or a combination of butterfly-like and loop-like owing to the different volatile and nonvolatile strain effect provided by PMN-PT substrate [25,26], as shown in Fig. S1 (Supplementary material S1). The change of magnetization behaves volatile for the butterfly-like case (Fig. S1a), while nonvolatile magnetization has been demonstrated for the other two cases. The change of magnetization can be entirely remained for the loop-like (Fig. S1b) and partially remained for the partial-loop-like case (Fig. S1c). Previous studies have revealed that the strain in FeRh film owing to substrate can totally determine the fractions of the coexisting AFM and FM phases [27,28] in the absence of magnetic field. A compressive/tensile strain favors the AFM/FM phase noting the ~1% volume difference between AFM and FM. Initially, AFM phase dominates the FeRh thin film and only a little FM phase coexists, as shown in Fig. 1a ①. The cycle starts with applying a magnetic field *H* (from ① to ②), resulting in the conversion of AFM to FM phase (②), which cools the film and absorbs heat from an external source. Then, a pulse electric field 0 ~ -*E* ~ 0 is applied across the thickness direction of the PMN-PT substrate to switch (②-③) and memorize (③-④) the strain state at a constant magnetic field *H*. Specifically, during 0 ~ -*E* (②-③), a compressive strain is produced which favors AFM phase and reduces the magnetization, and the strain is memorized and hence the magnetic state keeps the same during -*E* ~ 0 (③-④). The magnetic field *H* is then removed (from ④ to ⑤), resulting in the conversion of FM to AFM phase (⑤), which warms the film and releases heat to the external source. During the next ⑤-⑥-①, a pulsed electric field 0 ~ +*E* ~ 0 is applied across the PMN-PT substrate to recover the initial strain and magnetic state at zero magnetic field. Specifically, during 0 ~ +*E* (⑤-⑥), the compressive strain is released, which favors FM phase and increases the FM proportion, as a result, the magnetic state completely recovers to the initial state, while during +*E* ~ 0 (⑥-①) the strain and magnetic state is maintained owing to the strain memory effect. Fig. 1b clearly shows the reduction of hysteresis loss during the cycle mentioned above (cycle c-d compared to cycle a-b). Cycle a-b represents the one after the virgin cycle [13], which decreases a lot when a pulse *E* is simply applied at the points of magnetic field *H* and 0 (cycle c-d). The corresponding *M-E* and *M-T* curves are shown in Fig. 1c and Fig. 1d, respectively. All the relevant states labeled by the circled numbers in the refrigeration cycle (Fig. 1a) are correspondingly marked in the *M-H*, *M-E* and *M-T* curves.

3.2. Experimental verification of refrigeration cycle

To verify the refrigeration cycle stated above, a FeRh film about 50 nm-thick was grown on (011)-oriented (1-x)PMN-xPT single crystal substrate (x = 0.30). Fig. 2a shows the temperature dependent magnetization (*M-T* curve) measured at a magnetic field of 0.5 T along in-plane [100] direction with and without an electric field of − 6 kV cm^{-1} for FeRh/(011)PMN-PT. The transition temperature, T_0, in heating process locates at 368 K (the maximum of d*M*/d*T* under 0.5 T) in the absence of electric field, which is higher than that of the bulk owing to the compressive stress introduced by the lattice mismatch between FeRh and PMN-PT, analogous to the pressure experiments in bulk FeRh [29,30]. Magnetic field favors FM phase and a 5 T magnetic field shifts

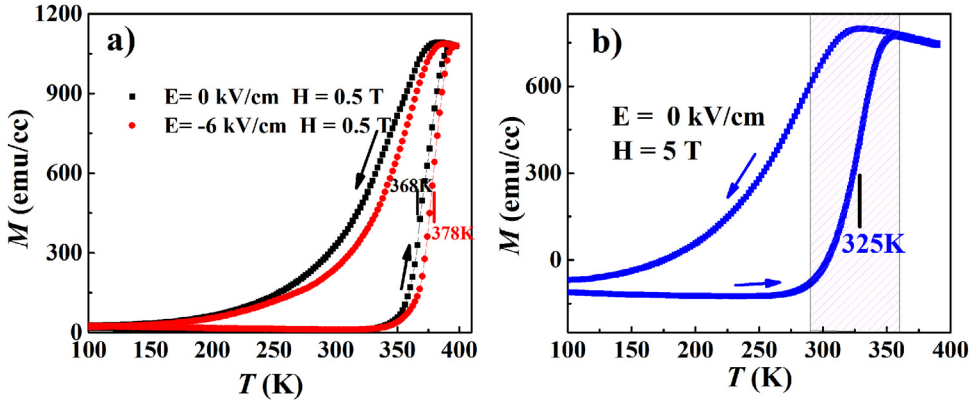

Fig. 2. (a) The *M-T* curves with and without application of − 6 kV cm^{-1} measured at 0.5 T. (b) The *M-T* curve at a high magnetic field of 5 T, where the shadow area signifies the phase transition region on heating.

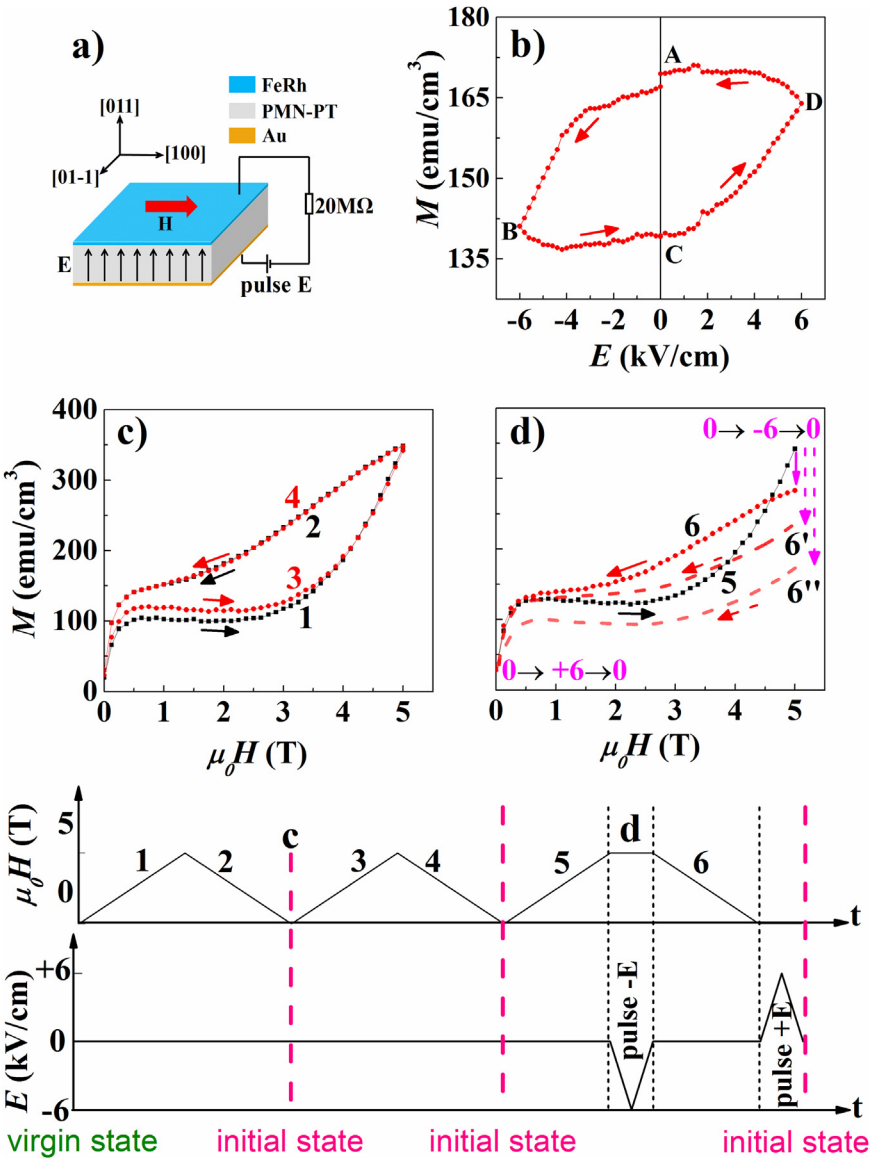

Fig. 3. (a) Sketch of the FeRh/PMN-PT heterostructure, where H and E denote the applied magnetic field and pulse electric field, respectively. (b) The loop-like M-E curve measured at 5 T and 310 K. (c) M-H curves in the virgin (path 1–2) and second (path 3–4) cycles in the absence of electric field, after that (d) path 5 from 0 to 5 T was continued and a pulse electric field 0 → − 6 → 0 kV cm^{-1} was applied to switch and memory the strain state at 5 T, then path 6 from 5 T to 0 was performed and followed by a pulse electric field 0 → + 6 → 0 kV cm^{-1}. Supposing the produced strain during 0 → − 6 → 0 kV cm^{-1} could be larger, path 6 would be along path 6′ or path 6″ instead, and then the enveloped area by path 5–6′ or 5–6″ would approach zero or turn out to be inverse. Lower panel, an exploded diagram corresponds to the above processes.

T_0 down to 325 K, as shown in Fig. 2b, where the shadow area denotes the phase transition region on heating. The thermal hysteresis of film, about 37 K, is broader than that of the bulk alloy because of the possibly introduced crystalline defects and chemical disorder during film growth [31]. With an applied electric field of − 6 kV cm^{-1}, the shape of M-T curves remains nearly unchanged while the transition temperature, T_0, shifts to a higher temperature by 10 K owing to the compressive stress transferred from the substrate.

We found that strain memory effect and loop-like M-E curve (magnetization as a function of electric field) can be constructed for the PMN-PT substrates with composition near the morphotropic phase boundary (MPB), where the electric field induced R-O phase transformation exerts substantial effect. The sketch of FeRh/PMN-PT heterostructure with the circuit of applying electric field is given in Fig. 3a. As a representative display, Fig. 3b shows the loop-like M-E curve measured at 5 T and 310 K.

To illustrate the reduction of hysteresis loss by utilizing strain memory effect for the FeRh/PMN-PT(011) heterostructure, we measured the isothermal magnetization as a function of magnetic field (M-H curves). The pulse electric field was applied along out of plane [011] while magnetic field along in-plane [100] direction, as shown in Fig. 3a. Before the M-H measurements at each temperature, FeRh film was cooled down to 100 K to ensure the sample at AFM phase, and then heated to the target temperature without magnetic field and electric field. M-H curves were measured at temperatures within the transition region (see the shadow area in Fig. 2b), and similar phenomena were observed. As a representative display, we choose 320 K to illustrate the manipulation on hysteresis loss, as shown in Fig. 3. For clarity, an exploded diagram is also given in the lower panel of Fig. 3.

The M-H loops exhibit a difference between the cycles 1–2 and 3–4 (Fig. 3c) due to the virgin effect [32] (see Supplementary material S2, Fig. S2). The main difference appears between the paths 1 and 3, while the paths 2 and 4 almost coincide, consistent with previous studies [32]. After these two cycles, we continue path 5 from 0 to 5 T in the absence of electric field (Fig. 3d). When the magnetic field reaches 5 T, a pulse electric field 0 → − 6 → 0 kV cm^{-1} is applied so as to switch and memorize the strain state. During 0 → − 6 kV cm^{-1}, the ferroelastic domain transformation of PMN-PT substrate produces a compressive strain, which favors AFM phase of FeRh films and leads to a drop of magnetization, as indicated by the magenta arrow in Fig. 3d (corresponding ②-③ in Fig. 1a). While during − 6 → 0 kV cm^{-1}, the ferroelastic domain does not switch to the original state and the strain is holding on a compressive state, i.e. strain memory effect, hence the magnetization keeps the same (③-④ in Fig. 1a). Then, path 6 from 5 T to

Table 1
Manipulation of hysteresis loss (W_{HL}) at temperatures within the transition region.

Temperature/K		310	315	320	325	330	340	350	360
Hysteresis loss (W_{HL}) /J kg^{-1}	cycle 3–4	16	23	34	48	66	111	118	85
	cycle 5–6	7	10	14	21	30	45	51	44
Reduction of W_{HL}/J kg^{-1} (compare cycle 5–6 to 3–4)		9	13	20	27	36	66	67	41
Reduced ratio of W_{HL} (compare cycle 5–6 to 3–4)		56%	57%	58%	56%	55%	59%	57%	48%

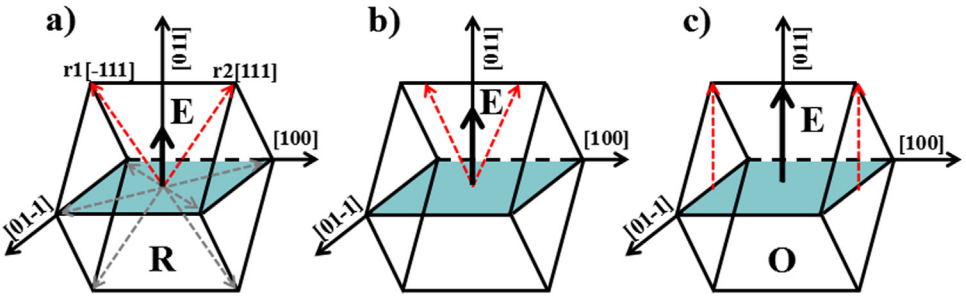

Fig. 4. The evolution of domain structure during the R-O phase transition for the PMN-PT single crystal with electric field E poled along [011] direction. (a) The arrows along the body diagonals denote the eight possible spontaneous polarization directions of R phase. The red arrows represent the polarization directions for (a) R phase, (b) intermediate phase, and (c) O phase.

0 is carried out (Fig. 3d). When the magnetic field returns zero, a pulse electric field 0 → + 6 → 0 kV cm^{-1} is applied to release the compressive strain, and make the system recover the initial strain state (⑤-⑥-① in Fig. 1a). Compared Fig. 3d to Fig. 3c, one can notice the large reduction of hysteresis loss (W_{HL}: the difference in area $\int MdH$ between *M-H* curves with increasing and decreasing *H*). Path 5 almost coincides with path 3, but the magnetization in the entire path 6 drops a lot compared to path 4 because the memorized compressive strain favors AFM state. At 320 K, the enveloped area by the cycle 3–4 is 34 J kg^{-1}, while the enveloped area by the cycle 5–6 becomes 14 J kg^{-1}, which reduces 58% compared to cycle 3–4. Table 1 summarizes the hysteresis loss and its manipulation at representative temperatures. One can see that the regulating ratio of hysteresis loss keeps almost the same within the transition region and the reduction ratio can be as much as ~56% in average when comparing the cycle 5–6 to 3–4.

Moreover, if the compressive strain generated during the 0 → − 6→ 0 kV cm^{-1} could be larger, the magnetization along the entire path 6 will further drop like path 6′ or path 6″ (Fig. 3d). As a result, the hysteresis loss may vanish or even become inverse, noting that the enveloped area by cycle 5–6′ approaches zero while the area by cycle 5–6″ is completely inverse. This phenomenon indicates that the elastic work done by strain effect counteracts hysteresis loss and saves the magnetic work. Not only the total hysteresis loss is canceled, the exceeding part will converts into heat energy, resulting in a novel enhancement of effective refrigeration capacity (RC_{effe}).

RC of FeRh film was evaluated based on magnetic entropy change ΔS, which was calculated based on the *M-H* data in the branch with *H* increasing. Note that the *M-H* curves with *H* increasing remains nearly unchanged for the cases with and without the pulse ± *E* (see Fig. 3c and d, the path 5 almost coincides with path 3). To ensure the reliable evaluation of ΔS, the well accepted loop method was used during the *M-H* measurements [33]. The FeRh film was firstly cooled down to 100 K before each *M-H* curve, and second-round data were adopted to avoid virgin effect. The resulted ΔS peaks at 343 K with a maximal value about 160 mJ cm^{-3} K^{-1} (see Fig. S3 in Supplementary material S3), and the evaluated RC is about ~376 J kg^{-1} according to $RC = \int_{T_1}^{T_2} |\Delta S_M(T)| dT$, where T_1 and T_2 are the temperatures corresponding to the half maximum of ΔS peak [34] and the mass density $\rho = 9760 kg/cm^3$ [22] of FeRh film is used. After deducting the maximal hysteresis loss, W_{HLmax} ~118 J kg^{-1}, the effective RC_{effe} ~258 J kg^{-1} counts 68% of RC for the case without pulse ± *E* [23]. However, with the application of pulse ± 6 kV cm^{-1}, the maximal W_{HLmax} reduces to ~51 J kg^{-1} and the corresponding RC_{effe} ~325 J kg^{-1} increases to 86% of RC. Moreover, this ratio RC_{effe}/RC could be further increased and reach a new height (exceeding 100%) if the compressive strain produced by the pulse -*E* could be further strengthened through designing the composition and engineering ferroelectric domain of the PMN-PT substrates.

4. Discussion

4.1. Strain memory effect

The strain memory effect and piezoelectric response in (1-x)PMN-xPT single crystals crucially depend on the multi-domain structure and the poled direction by electric field [35]. Generally, PMN-PT single crystal with rhombohedral structure has 8 spontaneous polarizations along the body diagonals, < 111 > orientations (Fig. 4a) [36]. When the PMN-PT is poled along [001] direction, strain memory effect can be realized along the in-plane [110] or [1–10] direction through 109° polarization switching [37]. While for the [011]-poled PMN-PT, 71° switching from out-plane to in-plane upon unipolar action can also lead to a strain memory effect [38]. However, the 109 ° switching contributed to the nonvolatility counts only 26% of the total for the [001] poled case, and the produced nonvolatile compressive strain is usually small, in average below − 0.05% [37]. Although 90% of switching (71° and 109 °) can be found in the [011]-poled case upon unipolar action, the produced compressive strain (~ −0.02% [36]) along [100] direction is also rather small (though a large tensile strain (0.13–0.25%) occurs along [01 − 1] direction [36,38]). A sufficient compressive stress is required to favor AFM phase of FeRh film and reduce its hysteresis loss. Here, we propose to utilize the large nonvolatile compressive strain (up to −0.45%) induced along in-plane [100] owing to irreversible rhombohedral-to-orthorhombic (R-O) phase transformation for (1-x)PMN-xPT single crystals with composition (x = 0.28–0.32) near the MPB. Generally, un-poled PMN-PT single crystal stays at a metastable multi-domain R phase with 8 spontaneous polarizations along the body diagonals. A negative electric field poled along the [011] direction switches the 8 equivalent ferroelectric domains from < 111 > polar axis into two crystal variants along [−111] and [111], as shown by red arrows in Fig. 4a. With further increasing electric field to a critical value, these two variants will rotate towards the [011] electric field direction (Fig. 4b), inducing a large shrink of [100] length and a structural transition from R to a single domain O phase (Fig. 4c).

The numerical value of strain relevant to R-O phase transition in (1-x)$Pb(Mg_{1/3}Nb_{2/3})O_3$-(x)$PbTiO_3$ (PMN-PT) single crystals crucially depend on the specific compositions. Different strains (up to −0.45%) and critical electric fields driving R-O phase transition have been

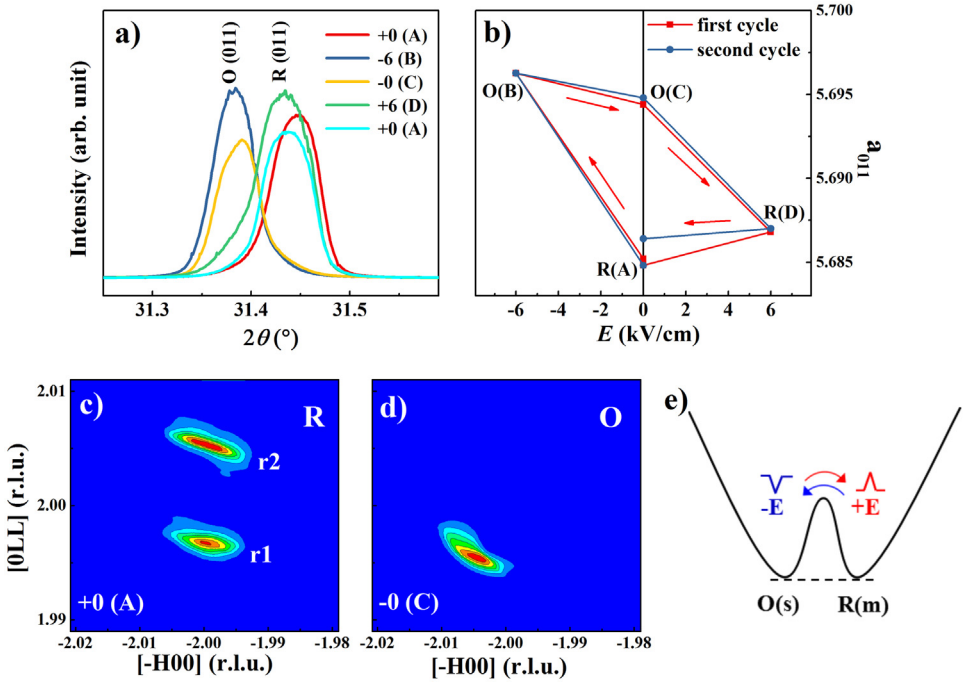

Fig. 5. (a) XRD patterns measured at room temperature, where the electric field E was in situ applied in the sequence of + 0, − 6, − 0, + 6, + 0 kV cm^{-1}. (b) The deduced lattice parameter a_{011} along the out-plane [011] direction versus E. Reciprocal space maps (RSMs) around the (−222) reflection of PMN-PT substrate for states of (c) + 0 and (d) − 0 kV cm^{-1}, where r1, r2 denote the domains of R phase. (e) Hypothetical Gibbs free energy profiles of multidomain R phase (R(m)) and single-domain O phase (O(s)). R, O denote rhombohedral and orthorhombic phase, respectively, while A, B, C, D in the brackets correspond to the ones in Fig. 3b.

observed for the PMN-PT single crystals with compositions near the MPB [39]. The change of PT concentration will alter the occupation of *B*-cite cations in the FE ABO_3 structure, leading to the displacements of both cations and anions. These ions occupy different types of orbitals and a hybrid bonding is typical due to the large number of preferred coordination geometries. The hybrid between *B*-site cations and O^{-2} lowers the bonding energy of BO_6, hence distorts the octahedron and domain structures, leading to various strains by electric field depending on PT concentration [40]. For x > 0.30, irreversible R-O phase transition tends to occur. O phase remains after removing electric field, signifying strain memory effect [39], but it returns to R phase upon an application of reverse electric field, which elongates the [100] length and converts O into R phase.

The commercial substrate with nominal composition x = 0.30 near MPB is adopted in present work. Under bipolar application of ± 6 kV cm^{-1} along [011] direction, we detected the structural transition from R to O phase and the strain memory effect, exactly corresponding to the loop-like *M-E* curve shown in Fig. 3b. Fig. 5a shows x-ray diffraction (XRD) patterns measured at room temperature, where the electric field was in situ applied in the sequence of + 0, − 6, − 0, + 6, + 0 kV cm^{-1}. The deduced lattice parameter a_{011} along the out-plane [011] for the pseudo-cubic R and O phases is shown in Fig. 5b. Significant extension along [011] appears upon the R to O phase transition, and more importantly memory effect is demonstrated. The R phase appears at + 0 kV cm^{-1} and transforms into O phase at − 6 kV cm^{-1}, which remains when the − 6 kV cm^{-1} is removed. Then an application of + 6 kV cm^{-1} makes the O phase return to R phase, which also remains when the + 6 kV cm^{-1} is removed, strongly evidencing the memory effect. We notice that the lattice elongates by about ~0.17% along the out-plane [011] direction upon switching from + 0 (point A) to − 0 state (point C). Repeated measurements demonstrated consistent results (see the first and second cycles in Fig. 5b).

To further understand the R-O transition and get information of in-plane lattice change along [100] direction, reciprocal space maps (RSMs) were measured around the (−222) reflection of PMN-PT substrate for the states + 0 (point A) and − 0 (point C) produced by the pulse ± 6 kV cm^{-1}. The results are shown in Fig. 5c and d, respectively. The two spots at + 0 state correspond to r1 and r2 polarization domains of R phase (Fig. 5c, Fig. 4a), which switch into a single spot at − 0 state corresponding to O phase (Fig. 5d, Fig. 4c). Since the in-plane reciprocal vector components of reflections around the (−222) peak are parallel to the [100] direction, the lattice parameter along in-plane [100] direction can be deduced from the RSMs. Accordingly, a compressive strain as large as ~ − 0.2% along in-plane [100] direction has been deduced as the + 0 state switched into − 0 state, which transferred to the FeRh film and hence produced the loop-like *M-E* and the different remanent magnetic states at + 0 (point A) and − 0 (point C), as shown in Fig. 3b. Accordingly, the estimated tensile stain along in-plane [01−1] direction is as small as 0.04% considering the tensile stain (0.17%) along out-plane [011] and the constantness of lattice volume. Moreover, one can notice that, from Fig. 3b and Fig. 5b, both the O and R phases of PMN-PT single crystal can equivalently exist at zero electric fields. In other words, the Gibbs free energy of the single domain O phase should be at the same level as that of the multi-domain R phase (Fig. 5e). It means that the motivation energy of pulse + 6 or − 6 kV cm^{-1} can equivalently drive the PMN-PT across the energy barrier between the R and O phases, leading to the strain memory effect and hence the nonvolatile control of hysteresis loss.

4.2. Evaluation of mechanical work

It is a universal law that energy cannot be created or destroyed. The reduction of hysteresis loss should be contributed by mechanical work in the elastic cycle, which saves the magnetic work and compensates the reduction of cooling efficiency caused by hysteresis loss, W_{HL}. Fig. 6a schematically displays the comparison of magnetic loops with and without the applications of pulse ± *E*. The shaded area denotes the difference of the two loops, i.e. the reduction of W_{HL}. Fig. 6b displays the schematic of mechanical work, W_{mech}, during an elastic cycle (see the shadow area), where the thin film stress σ versus in-plane strain ε_{FeRh} is schematically shown. Based on the measured compressive strain (−0.20%) along the in-plane [100] direction, mechanical work, W_{mech}, in the elastic cycle can be evaluated according to the following relation,

$$W_{mech} = \frac{1}{m} \cdot V \oint \sigma \cdot d\varepsilon \quad (1)$$

where *m* is the mass of FeRh film, *V* the volume of FeRh film, the stress induced by magnetic field, and the in-plane strain (−0.20%) along

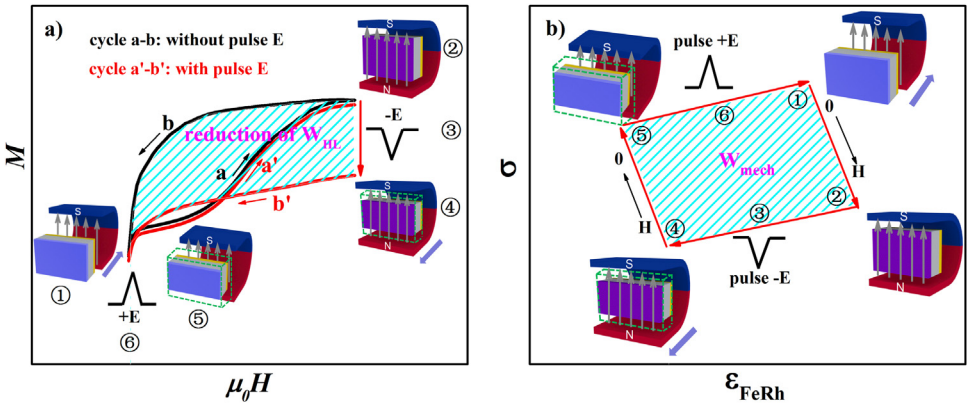

Fig. 6. Schematic of (a) the magnetic loops with (path a′-b′) and without (path a-b) the applications of pulse ± *E*, and (b) mechanical work (the shadow area), W_{mech}, during the refrigeration cycle, where the thin film stress σ versus in-plane strain ε_{FeRh} is schematically shown. The cycled numbers correspond to the ones shown in Fig. 1.

[100] induced by a pulse electric field. Here, the stress $\sigma = B\varepsilon_{AFM-FM}$ is estimated based on the linear strain ($\varepsilon_{AFM-FM} = 0.3\%$[18]) produced during the transition from AFM to FM, and the elastic modulus $B = 2.05 \times 10^{11}$Pa of FeRh is adopted [41]. The resulted mechanical work is $W_{mech} \sim 126\,J\,kg^{-1}$. Noting the maximal reduction of W_{HL} is $\sim 67\,J\,kg^{-1}$ (see Table 1), about 53% of W_{mech} compensates the W_{HL} while the rest is for self-loss. Supposing this ratio for compensating keeps unchanged, the maximal hysteresis loss ($W_{HL} \sim 118\,J\,kg^{-1}$, Table 1) can be completely compensated as the produced strain reaches − 0.35%, noting that the W_{mech} is proportional to the strain caused by pulse ± *E* from Eq. (1). Accordingly, the W_{mech} for compensation will exceed the maximal W_{HL} as long as the strain is over − 0.35%. The excess part converts into heat energy, leading to a novel enhancement of cooling efficiency by utilizing mechanical work. That is $RC_{effe} > RC$, as stated above. Previous literature [38] indicates that the numerical value of strain relevant to R-O phase transition in (1-x)Pb($Mg_{1/3}Nb_{2/3}$)O_3-(x)$PbTiO_3$ (PMN-PT) single crystals can be up to − 0.45%, crucially depending on the compositions [39].

4.3. Evaluated COP in an ideal magnetic refrigeration cycle

COP (coefficient-of-performance) is a fundamental parameter reflecting cooling efficiency in a magnetic refrigeration cycle. For better understanding the role of mechanical work in compensating hysteresis loss in a magnetic refrigeration cycle, we take the ideal magnetic Carnot cycle as an example and evaluated the COP. An ideal magnetic Carnot cycle between hot and cold baths composes of two isothermal and two adiabatic processes, as shown in the entropy-temperature (*S*-*T*) diagram of FeRh (Fig. 7), where T_h (A,D) and T_c (B,C) represent the temperatures of hot and cold baths, respectively. Magnetizing and demagnetizing are both accomplished in two sub processes. In the *adiabatic process* from A to B, the cycle starts from the initial state A at temperature T_h of the hot bath with $H_A = 0$. With adiabatically increasing magnetic field to H_B, the temperature of FeRh decreases to the T_c of the cold bath (inverse MCE). While in the *isothermal process* from B to C, FeRh is set in thermal contact with and absorbed heat from the cold bath, and the magnetic field is further increased to the maximal H_C at the point of C. Then in another *adiabatic process* from C to D, the magnetic field adiabatically decreases to H_D and the temperature returns to T_h. In the *isothermal process* from D to A, FeRh is set in thermal contact with and released heat to the hot bath, and the magnetic field decreases to the initial state $H_A = 0$. In these adiabatic processes, entropy does not remain constant because W_{HL} acts as an unavoidable entropy source [42]. For simplicity, the impact is only denoted in the C-D branch.

Here, we consider an ideal magnetic Carnot cycle with a hot reservoir at $T_h = 343$ K (the peak temperature of Δ*S*) and a temperature span (T_h-T_c) = 8.5 K for FeRh [17]. COP is normally bounded by the Carnot limit [9], i.e. $COP_{Carnot} = T_c/(T_h\text{-}T_c) = 39.4$ (Fig. 7a), where the both magnetic hysteresis loss and external mechanical work are not taken into account. From the perspective of energy, the COP of carnot cycle is determined by the ratio of the heat absorbed from the cold reservoir and the work done to the refrigerant, and the COP can be described as $COP_{Carnot} = Q/W_{Carmot}$. $Q = T|\Delta S|$ is evaluated based on the peak value and position of Δ*S* (Fig. S3b). Substituting these corresponding values into the formula, the value of $W_{Carmot} = 143\,J\,kg^{-1}$ can be obtained. When the hysteresis loss is taken into account (Fig. 7b), the work needed must increase if the heat absorbed from the cold reservoir remains unchanged. Therefore, the COP becomes smaller than the COP_{carnot}. In this paper, the maximal hysteresis loss (additional magnetic work) $W_{HL} \sim 118\,J\,kg^{-1}$ (Table 1) in FeRh film would lead to $COP = Q/(W_{HL} + W_{Carnot}) = 21.5$, which is about 54% of the Carnot efficiency (Fig. 7b), corresponding to the effective refrigeration capacity $RC_{effe} \sim 258\,J\,kg^{-1}$ ~68% of RC as stated above. If the hysteresis loss was partially (Fig. 7c) or completely compensated (Fig. 7d) by W_{mech}, the W_{HL} would reduce to $\sim 51\,J\,kg^{-1}$ or $0\,J\,kg^{-1}$ upon the cooperation of strain memory effect of − 0.20% or − 0.35% by a pulse ± *E*, and the COP would increase to 29.0 or 39.4(full Carnot limit), corresponding to 74% or 100% of the Carnot efficiency, and $RC_{effe}/RC \sim 86\%$ or 100% respectively. With further increasing the W_{mech} by strengthening the strain ($> |-0.35\%|$), the W_{HL} would become inverse (negative), leading to the result $COP > COP_{Carnot}$ (Fig. 7e) and $RC_{effe}/RC > 100\%$. These relations tell us the ideal COP or RC_{effe} in a magnetic Carnot cycle can increase to a new height through introducing external mechanical work. It should be noted that, for simplicity, the ideal magnetic carnot cycle here only considers the effect of magnetic hysteresis loss in FeRh films and the mechanical work done on the films. In a real device, the COP would be also affected by other losses, such as the ferroelectric losses in the substrate, but they can themselves be reduced by optimization. The relation $COP > COP_{Carnot}$ here only denotes the fundamental enhancements of RC_{effe} by utilizing mechanical work.

4.4. Inverse hysteresis loss

Although an inverse hysteresis loss was not experimentally observed yet in FeRh film by utilizing non-volatile strain provided by anisotropic (011)-PMN-PT substrates, the inverse hysteresis loss would appear as long as the strain could be large enough through engineering ferroelectric domain of the PMN-PT substrates. In order to prove the possibility of inverse hysteresis loss, we do achieve the inverse hysteresis loss in the FeRh film grown on (001)-cut PMN-PT substrates, as shown in Fig. 8, where the electric field, $-8\,kV\,cm^{-1}$, is continuously applied during the demagnetization process. As the $-8\,kV\,cm^{-1}$ is applied along out-plane [001] direction, the produced isotropic in-plane compressive strain, analogous to hydrostatic pressure, favors AFM phase of FeRh films and causes a large drop of magnetization. As a result, inverse hysteresis loss appears. Although the change of the hysteresis loss in

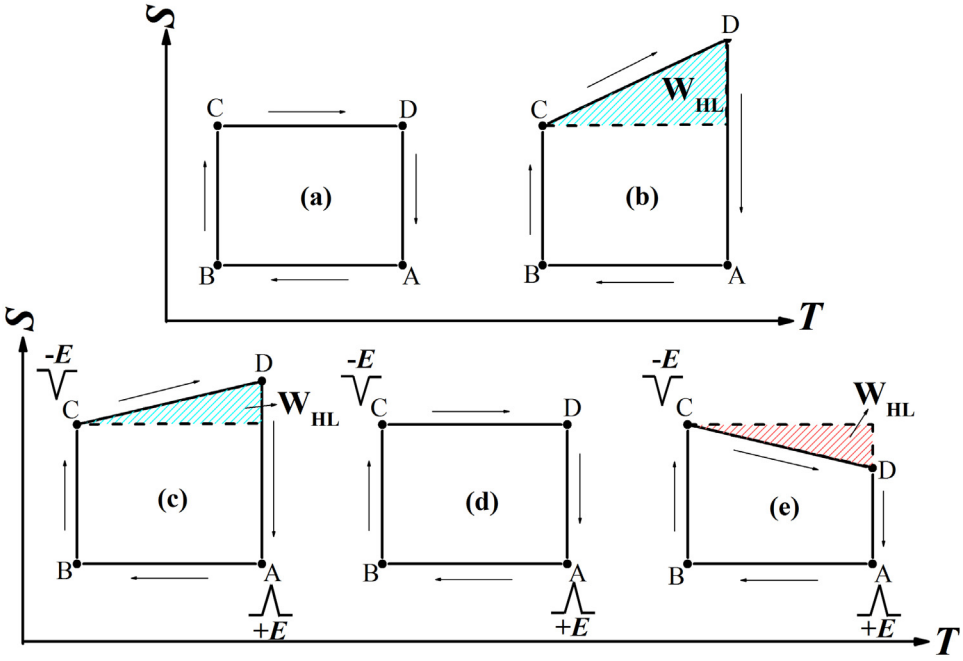

Fig. 7. *S-T* diagram of FeRh for an ideal magnetic Carnot cycle between T_h (A,D) and T_c (B,C) composed of two isothermal and two adiabatic processes: (a) Reversible Carnot cycle without considering hysteresis loss; (b) Carnot cycle considering full W_{HL} without pulse ± *E*; (c) Carnot cycle considering partially reduced W_{HL} with pulse -*E*, + *E* successively applied at points C, A; (d) Carnot cycle considering fully reduced $W_{HL} = 0$ with pulse ± *E*; (e) Carnot cycle considering inverse hysteresis loss, $W_{HL} < 0$, with pulse ± *E*. In the adiabatic processes, entropy does not remain constant because W_{HL} acts as an unavoidable entropy source [42]. For simplicity, the impact is only denoted in the C-D branch.

this case relies on the electric field, which is volatile and disappears when the electric field is removed, the appearance of inverse hysteresis loss proves the possibility of $RC_{effe}/RC > 100\%$ by utilizing mechanical work, and the ideal $COP > COP_{Carnot}$ if only hysteresis loss and the contribution of mechanical work were considered. Desired ferroelastic properties and strain effect can be reached through domain engineering for the FE substrates.

5. Conclusion

In summary, we have solved the fatal problem of large hysteresis loss in FeRh, which seriously harms cooling efficiency. Nonvolatile reduction of hysteresis loss is realized by utilizing the large strain memory effect provided by R-O phase transformation of [011] bipolar PMN-PT substrate. The application of electric field is avoided during heat absorb/release (magnetization/demagnetization) process, which solves the bottleneck problem in designing dual field cycle in a prototype. Mechanical work produced owing to elastic strain compensates hysteresis loss and saves the magnetic work. Quantitative analysis indicates that the effective refrigeration capacity (RC_{effe}) can increase to a new height by utilizing external mechanical work as long as the nonvolatile strain can be large enough, and the ideal COP would exceed Carnot limit if only hysteresis loss and the contribution of mechanical work were considered. This fundamental advance opens a new avenue for enhancing refrigeration efficiency by utilizing mechanical work. The feasibility of proposed refrigeration cycle with the cooperation of strain memory effect not only helps rescuing the FeRh as a magnetic refrigerant but also paves a new way to solve large hysteresis loss for similar caloric materials.

Acknowledgements

We thank Dr. Jun Lu for the discussion about finite element simulation. We are also grateful to Shanghai Institute of Applied Mathematics and Mechanics for the help of finite element simulation. This work was supported by the National Key Research and Development Program of China (Grant Nos. 2017YFB0702702, 2018YFA0305704, 2017YFA0303601, 2017YFA0206300, 2016YFB0700903), the National Natural Science Foundation of China (Grant Nos. 51531008, U1832219, 51771223, 51590880, 11674378), and the Key Program and Strategic Priority Research Program (B) of the Chinese Academy of Sciences.

Competing financial interests

The authors declare no competing financial interests.

Appendix A. Supplementary material

Supplementary data associated with this article can be found in the online version at doi:10.1016/j.nanoen.2019.02.044.

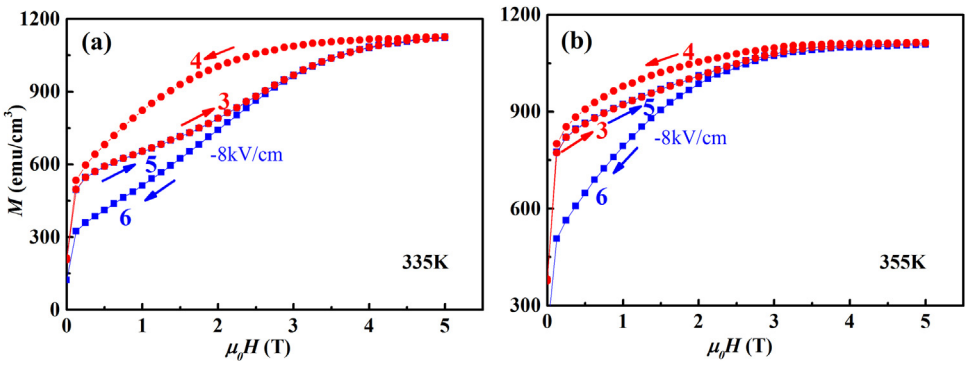

Fig. 8. Realization of an inverse hysteresis loss with electric field applied during the demagnetization process at 335 K (a) and 355 K (b). Path 3–4 denotes the *M-H* curve in the absence of electric field in the second cycle (the virgin effect has been eliminated, and path 1–2 does not show for clarify), while Path 5–6 denotes the subsequent cycle, where $-8\,kV\,cm^{-1}$ is applied in the entire demagnetization process. One can notice the inverse hysteresis cycled by Path 5–6.

References

[1] European Union on Climate Action giving the Paris Agreement on the Climate conference (COP21). 〈https://ec.europa.eu/clima/policies/international/negotiations/paris_en〉.

[2] V.K. Pecharsky, K.A. Gschneidner Jr, The giant magnetocaloric effect in $Gd_5(Si_2Ge_2)$, Phys. Rev. Lett. 78 (1997) 4494–4497.

[3] B.L. Peng, Q. Zhang, Y.N. Lyu, L.J. Liu, X.J. Lou, C. Shaw, H.T. Huang, Z.L. Wang, Thermal strain induced large electrocaloric effect of relaxor thin film on LaNiO3/Pt composite electrode with the coexistence of nanoscale antiferroelectric and ferroelectric phases in a broad temperature range, Nano Energy 47 (2018) 285–293.

[4] B. Neese, B. Chu, S.G. Lu, Y. Wang, E. Furman, Q.M. Zhang, Large electrocaloric effect in ferroelectric polymers near room temperature, Science 321 (2008) 821–823.

[5] T. Jaka, E. Kurt, E. Dan, D. Stefano, T. Janez, P. Nini, A regenerative elastocaloric heat pump, Nat. Energy 1 (2016) 16134.

[6] X. Moya, S. Kar-Narayan, N.D. Mathur, Caloric materials near ferroic phase transitions, Nat. Mater. 13 (2014) 439–450.

[7] L. Mañosa, A. Planes, Materials with giant mechanocaloric effects: cooling by strength, Adv. Mater. 29 (2017) 1603607.

[8] O. Tegus, E. Brück, K.H.J. Buschow, F.R. de Boer, Transition-metal-based magnetic refrigerants for room-temperature applications, Nature 415 (2002) 150–152.

[9] Y. Liu, Lee C. Phillips, R. Mattana, M. Bibes, A. Barthelemy, B. Dkhil, Large reversible caloric effect in FeRh thin films via a dual-stimulus multicaloric cycle, Nat. Commun. 7 (2016) 11614.

[10] B.G. Shen, J.R. Sun, F.X. Hu, H.W. Zhang, Z.H. Cheng, Recent progress in exploring magnetocaloric materials, Adv. Mater. 21 (2009) 4545–4564.

[11] Y.Y. Gong, D.H. Wang, Q.Q. Cao, E.K. Liu, J. Liu, Y.W. Du, Electric field control of the magnetocaloric effect, Adv. Mater. 27 (2015) 801–805.

[12] F.X. Hu, B.G. Shen, J.R. Sun, Z.H. Cheng, G.H. Rao, X.X. Zhang, Influence of negative lattice expansion and metamagnetic transition on magnetic entropy change in the compound $LaFe_{11.4}Si_{1.6}$, Appl. Phys. Lett. 78 (2001) 3675–3677.

[13] A. Fujita, S. Fujieda, Y. Hasegawa, K. Fukamichi, Itinerant-electron metamagnetic transition and large magnetocaloric effects in $La(Fe_xSi_{12-x})_{13}$ compounds and their hydrides, Phys. Rev. B 67 (2003) 104416.

[14] J. Liu, T. Gottschall, K.P. Skokov, J.D. Moore, O. Gutfleisch, Giant magneto-caloric effect driven by structural transitions, Nat. Mater. 11 (2012) 620–626.

[15] L. Mañosa, D. Alonso, A. Planes, E. Bonnot, M. Barrio, J. Tamarit, S. Aksoy, M. Acet, Giant solid-state barocaloric effect in the Ni-Mn-In magnetic shape memory alloy, Nat. Mater. 9 (2010) 478–481.

[16] S.A. Nikitin, G. Myalikgulyev, A.M. Tishin, M.P. Annaorazov, K.A. Asatryan, A.L. Tyurin, The magnetocaloric effect in $Fe_{49}Rh_{51}$ compound, Phys. Lett. A 148 (1990) 363–366.

[17] M.P. Annaorazov, S.A. Nikitin, A.L. Tyurin, K.A. Asatryan, A. Kh. Dovletov, Anomalously high entropy change in FeRh alloy, J. Appl. Phys. 79 (1996) 1689–1695.

[18] A.I. Zakharov, A.M. Kadomtseva, R.Z. Levitin, E.G. Ponyatovskii, Magnetic and magnetoelastic properties of a metamagnetic iron–rhodium alloy, Sov. Phys. JETP 19 (1964) 1348–1353.

[19] A. Chirkova, K.P. Skokov, L. Schultz, N.V. Baranov, O. Gutfleisch, T.G. Woodcock, Giant adiabatic temperature change in FeRh alloys evidenced by direct measurements under cyclic conditions, Acta Mater. 106 (2016) 15–21.

[20] C. Bordel, J. Juraszek, D.W. Cooke, C. Baldasseroni, S. Mankovsky, J. Minar, H. Ebert, S. Moyerman, E.E. Fullerton, F. Hellman, Fe spin reorientation across the metamagnetic transition in strained FeRh thin films, Phys. Rev. Lett. 109 (2012) 117201.

[21] S.A. Nikitin, G. Myalikgulyev, M.P. Annaorazov, A.L. Tyurin, R.W. Myndyev, S.A. Akopyan, Giant elastocaloric effect in FeRh alloy, Phys. Lett. A 171 (1992) 234–236.

[22] E. Stern-Taulats, A. Planes, P. Lloveras, M. Barrio, J.L. Tamarit, S. Pramanick, S. Majumdar, C. Frontera, L. Mañosa, Barocaloric and magnetocaloric effects in $Fe_{49}Rh_{51}$, Phys. Rev. B 89 (2014) 214105.

[23] V. Provenzano, A.J. Shapiro, R.D. Shull, Reduction of hysteresis losses in the magnetic refrigerant $Gd_5Ge_2Si_2$ by the addition of iron, Nature 429 (2004) 853–857.

[24] J. Lyubina, R. Schafer, N. Martin, L. Schultz, O. Gutfeisch, Novel design of La $(Fe,Si)_{13}$ alloys towards high magnetic refrigeration performance, Adv. Mater. 22 (2010) 3735–3739.

[25] J.P. Han, W.W. Cao, Electric field effects on the phase transitions in [001]-oriented $(1-x)Pb(Mg_{1/3}Nb_{2/3})O_3$-$xPbTiO_3$ single crystals with compositions near the morphotropic phase boundary, Phys. Rev. B 68 (2003) 134102.

[26] Y. Liu, Y.G. Zhao, P.S. Li, S. Zhang, D.L. Li, H. Wu, A.T. Chen, Y. Xu, X.F. Han, S.Y. Li, D. Lin, H.S. Luo, Electric-field control of magnetism in $Co_{40}Fe_{40}B_{20}$/(1-x)Pb $(Mg_{1/3}Nb_{2/3})O_3$-$xPbTiO_3$ multiferroic heterostructures with different ferroelectric phases, ACS Appl. Mater. Interfaces 8 (2016) 3784–3791.

[27] Z.Q. Liu, L. Li, Z. Gai, J.D. Clarkson, S.L. Hsu, A.T. Wong, L.S. Fan, M.W. Lin, C.M. Rouleau, T.Z. Ward, H.N. Lee, A.S. Sefat, H.M. Christen, R. Ramesh, Full electroresistance modulation in a mixed-phase metallic alloy, Phys. Rev. Lett. 116 (2016) 097203.

[28] I. Fina, A. Quintana, J. Padilla-Pantoja, X. Martí, F. Macia, F. Sánchez, M. Foerster, L. Aballe, J. Fontcuberta, J. Sort, Electric-field-adjustable time-dependent magnetoelectric response in martensitic FeRh alloy, ACS Appl. Mater. Interfaces 9 (18) (2017) 15577–15582.

[29] L.I. Vinokurova, A. Vlasov, N. Kulikov, M. Pardavi-Horvath, Pressure-induced antiferromagnetism in ferromagnetic $Fe_{51.5}Rh_{48.5}$ alloy, J. Magn. Magn. Mater. 25 (1981) 201.

[30] A. Hernando, J.M. Barandiaran, J.M. Rojo, J.C. Gomez-Sal, About the effect of pressure and volume expansion on the transition from antiferromagnetic to ferromagnetic state in some metal alloys, J. Magn. Magn. Mater. 174 (1997) 181.

[31] S. Maat, J.-U. Thiele, E. Fullerton, Temperature and field hysteresis of the antiferromagnetic-to-ferromagnetic phase transition in epitaxial FeRh films, Phys. Rev. B 72 (2005) 214432.

[32] M. Manekar, S.B. Roy, Reproducible room temperature giant magnetocaloric effect in FeRh, J. Phys. D: Appl. Phys. 41 (2008) 192004.

[33] L. Caron, Z.Q. Ou, T.T. Nguyen, D.T. CamThanh, O. Tegus, E. Bruck, On the determination of the magnetic entropy change in materials with first-order transitions, J. Magn. Magn. Mater. 321 (2009) 3559–3566.

[34] K.A. Gschneidner Jr, V.K. Pecharsky, A.O. Pecharsky, C.B. Zimm, Recent developments in magnetic refrigeration, Mater. Sci. Forum 315 (317) (1999) 69–76.

[35] E.W. Sun, W.W. Cao, Relaxor-based ferroelectric single crystals: growth, domain engineering, characterization and applications, Prog. Mater. Sci. 65 (2014) 124–210.

[36] T. Wu, A. Bur, P. Zhao, K.P. Mohanchandra, K. Wong, K.L. Wang, C.S. Lynch, G.P. Carman, Giant electric-field-induced reversible and permanent magnetization reorientation on magnetoelectric Ni/(011) $[Pb(Mg_{1/3}Nb_{2/3})O_3]_{(1-x)}$-$[PbTiO_3]_x$ heterostructure, Appl. Phys. Lett. 98 (2011) 012504.

[37] S. Zhang, Y.G. Zhao, P.S. Li, J.J. Yang, S. Rizwan, J.X. Zhang, J. Seidel, T.L. Qu, Y.J. Yang, Z.L. Luo, Q. He, T. Zou, Q.P. Chen, J.W. Wang, L.F. Yang, Y. Sun, Y.Z. Wu, X. Xiao, X.F. Jin, J. Huang, C. Gao, X.F. Han, R. Ramesh, Electric-field control of nonvolatile magnetization in $Co_{40}Fe_{40}B_{20}$/$Pb(Mg_{1/3}Nb_{2/3})_{0.7}Ti_{0.3}O_3$ structure at room temperature, Phys. Rev. Lett. 108 (2012) 137203.

[38] M. Liu, B.M. Howe, L. Grazulis, K. Mahalingam, T.X. Nan, N.X. Sun, G.J. Brown, Voltage-impulse-induced non-volatile ferroelastic switching of ferromagnetic resonance for reconfigurable magnetoelectric microwave devices, Adv. Mater. 25 (2013) 4886–4892.

[39] M. Shanthi, L.C. Lim, Electric-field and stress-induced R-O phase transformation in [011]-poled $Pb(Mg_{1/3}Nb_{2/3})O_3$–(28–32)%$PbTiO_3$$Pb(Mg_{1/3}Nb_{2/3})O_3$–(28–32)% $PbTiO_3$ single crystals of [100]-length cut, J. Appl. Phys. 106 (2009) 114116.

[40] J. Peräntie, T. Correia, J. Hagberg, A. Uusimäki, Electrocaloric, Materials 34 (2014) 47.

[41] V.L. Moruzzi, P.M. Marcus, S.L. Qiu, Oscillatory magnetism in compounds of iron with 4d metals, Phys. Rev. B 52 (1995) (3488-3452).

[42] B. Vittorio, P.S. Carlo, B. Giorgio, L. Martino, Effect of material hysteresis in magnetic refrigeration cycles, Int. J. Refrig. 29 (2006) 1358–1365.

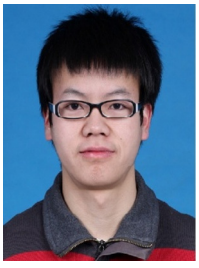

Kaiming Qiao is currently a Ph. D. candidate under the supervisor of Prof. Fengxia Hu at Institute of Physics, Chinese Academy of Sciences. His research interests focus on multi-field modulated magnetocaloric effect in first order phase transition materials and magnetic refrigeration application of thin films in microelectronic circuit.

Fengxia Hu is a Professor at Institute of Physics, Chinese Academy of Science since 2008. She received her Ph.D in Physics at Institute of Physics, Chinese Academy of Science in 2002 with major of condensed matter physics. Her current research interests focus on magnetocaloric and multicalorc effect, solid state refrigeration applications of various intermetallics and oxides, such as Fe-based $NaZn_{13}$-type materials, NiMn-based Heusler alloys, and etc. Current interest also includes the influence of polarization and strain induced by substrate on magnetic transport properties of ultrathin films.

Yao Liu received her Ph.D. from the Institute of Physics, Chinese Academy of Science. Her research interests include the room temperature magnetocaloric effect, multicaloric effect of ferroic materials with coupled nature of lattice and spin, and their applications in the solid state refrigeration.

Jia Li currently is pursuing his Ph.D. degree under the supervision of Prof. Feng-xia Hu at the Institute of Physics, Chinese Academy of Sciences. His research interests are spin order regulation under multiple fields and novel physical property of complex oxide films.

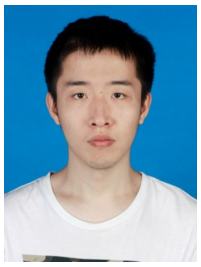

Hao Kuang is currently a postdoctoral associate in the group of Prof. Pu Yu in Tsinghua University. He received Ph.D. degree in condensed matter physics from the institute of physics, Chinese Academy of Sciences, in 2018 under the supervision of Prof. Feng-Xia Hu and associate prof. Jing Wang. His recent researches focus on designing functional oxide heterostructure, and finite element modelling.

Wen-Hui Liang received her B.S. degree in 2011 from College of Physics and Information Engineering, Hebei Normal University. She is currently a doctoral student in Institute of Physics, Chinese Academy of Sciences under the supervision of Prof. Feng-Xia Hu. Her research interests include the multiferrorics and regulated magnetism under multiple fields.

Hongrui Zhang received the M.S. degree in Hebei University. He is currently pursuing the Ph.D. degree at Institute of Physics, Chinese Academy of Science. His research is focusing on the regulated magnetism under multiple fields and spin-polarized two dimensional electron gases at oxide interface.

Jing Wang is currently an associate professor in Institute of Physics, Chinese Academy of Science. He received his Ph.D at Institute of Physics, Chinese Academy of Science in 2001. His current research interests focus on various caloric effects relating to order-disorder phase transitions and the combined effect of external multi-fields, the regulation effect of interface carrier doping, interlayer coupling, strain and ion-defects in strongly correlated electron systems.

Jirong Sun is a Professor of Condensed Matter Physics in Institute of Physics of the Chinese Academy of Sciences since 1999. He received his Ph.D.at Institute of Physics, Chinese Academy of Sciences in 1989. His current research interest focus on transport behavior of spin polarized electrons in oxides and fabrication, characterization of the heteroepitaxial multilayers of various perovskite oxides, and the effects of size, interface, intra- and interlayer coupling. Moreover, he has gained a lot of achievements in magnetocaloric effects in rare-earth and transition metals and alloys.

Baogen Shen is a Professor at Institute of Physics, Chinese Academy of Science since 1995. His current research interest focus on structure, magnetic properties and magnetocaloric effects of rare-earth-transition-metal compounds; microstructure and magnetic properties of rare earth permanent magnet.